Muon kinetics in heat treated Al(–Mg)(–Si) alloys

Sigurd Wenner[a], Katsuhiko Nishimura[b], Kenji Matsuda[b], Teiichiro Matsuzaki[c], Dai Tomono[c], Francis L. Pratt[d], Calin D. Marioara[e], Randi Holmestad[a]

[a] *Department of Physics, NTNU, Høgskoleringen 5, NO-7491 Trondheim, Norway*
[b] *Department of Materials Science and Engineering, University of Toyama, Gofuku 3190, Toyama-shi, Toyama 930-8555, Japan*
[c] *Advanced Meson Science Laboratory, RIKEN Nishina Center for Accelerator Based Science, RIKEN, Wako, Saitama 351-0198, Japan*
[d] *ISIS Facility, Rutherford Appleton Laboratory, Chilton OX11 0QX, United Kingdom*
[e] *Materials and Chemistry, SINTEF, Box 4760 Sluppen, NO-7465 Trondheim, Norway*

Abstract

Al–Mg–Si alloys are heat-treatable and rely on precipitation hardening for their mechanical strength. We have employed the technique of muon spin relaxation to further our understanding of the complex precipitation sequence in this system. The muon trapping kinetics in a material reveals a presence of atom-sized defects such as solute atoms (Mg and Si) and vacancies. By comparing the muon kinetics in pure Al, Al–Mg, Al–Si and Al–Mg–Si when held at different temperatures, we establish an interpretation of muon trapping peaks based on different types of defects. Al–Mg–Si samples have a unique muon trapping peak at temperatures around 200 K. This peak is highest for samples that have been annealed at 70–150 °C, which have microstructures dominated by a high density of clusters/GP-zones. The muon trapping is explained by the presence in vacancies inside these structures. The vacancies disappear from the material when the clusters transform into more developed precipitates during aging.

Keywords: Aluminium alloys, Muon spin relaxation, Vacancies, Precipitation

Email address: sigurd.wenner@ntnu.no (Sigurd Wenner)

1. Introduction

Muon spin methods are mainly used to probe magnetic properties of materials, but can also be used to study other phenomena as a *consequence* of their magnetic properties. A common example is solid state diffusion in non-magnetic materials [1]. The techniques are similar to positron annihilation spectroscopy (PAS) in that unstable elementary particles are implanted in a material, they decay, and their decay products are detected outside of the material. The spin precession of muons can be indirectly observed through the positrons they decay into. In a muon spin relaxation (μSR) experiment, muons enter the sample with their spin aligned antiparallel to their direction of motion. With no external field applied, the precession is caused by magnetic fields set up by the atomic nuclei inside the material. In a non-magnetic metal like aluminium, these fields are randomly oriented, and polarized muons become depolarized ("relaxed") in a matter of microseconds.

Al–Mg–Si alloys constitute most of the worldwide aluminium market as they have good mechanical strength and are easily formable into end products [2]. An optimal heat treatment of alloys containing merely 1 % solutes (Mg and Si) typically increases the hardness by a factor of 5 from pure aluminium. After the material is formed, an industrial hardening procedure consists of solution heat treatment (SHT), typically at 550 °C, some (unavoidable) storage at room temperature (RT), and artificial aging (AA), typically at 180 °C. The hardening during heat treatment is caused by precipitation of metastable phases through diffusional phase transitions. Going from low to high aging times/temperatures, the generic precipitation sequence for Al alloys is

$$\begin{aligned} \text{SSSS} &\rightarrow \text{Solute clusters} \rightarrow \text{Semi-coherent (hardening) precipitates} \\ &\rightarrow \text{Incoherent (non-hardening) precipitates,} \end{aligned} \tag{1}$$

where SSSS is an acronym for supersaturated solid solution. In general, the precipitate phases grow larger and become fewer as we proceed through the sequence.

Al–Mg–Si alloys quenched from SHT are unstable at RT, and atomic clusters (with Mg and Si at Al-fcc positions) form from the SSSS. The clusters in general are too small and coherent with the Al matrix to be observed by transmission electron microscopy (TEM). However, new experimental possibilities have sparked an interest in solute clustering the last decades, with techniques such as PAS [3, 4], APT [5, 6, 7] and differential scanning calorimetry (DSC) [8, 9]. Several independent atom probe tomography (APT) studies [5, 10]

have shown that two kinds of solute clusters can form in Al–Mg–Si alloys. Cluster(1) (the "bad" cluster) forms during RT storage (of alloys with Mg + Si $>$ 1 % [10, 11]), has a non-fixed composition and does not grow or develop during further heat treatment. Cluster(2) (the "good" cluster) forms during annealing at 70–150 °C directly after SHT [6] (and during RT storage of alloys with Mg + Si $<$ 1 % [10, 11]), has a Mg/Si ratio close to 1 and can develop into hardening β'' precipitates.

The hardening Al–Mg–Si precipitates are all needle-shaped with their main growth/coherency direction along $\langle 001 \rangle_{\mathrm{Al}}$. The most important of these is β'' [12, 13]. At temperatures above 200 °C, Al–Mg–Si alloys overage, transforming β'' to less coherent precipitates, which causes a drop in hardness. The thermal and mechanical treatments applied to alloys determine their progression through the precipitation sequence. Understanding the early steps, in particular the formation of Mg–Si(–vacancy) clusters, is essential as the composition, concentration, and size of these clusters influence the precipitate microstructure in finished products.

Muons undergo interstitial diffusion inside solids. In aluminium, they have been shown to be trapped by atoms in substitutional lattice positions and by vacancies [14, 15], yielding a lower apparent muon diffusivity. In this work, we exploit this effect and identify the muon trapping behavior of Mg and Si atoms as well as vacancies in different stages of heat treatment of aluminium alloys. Due to its industrial and scientific interest, we hereby study the ternary Al–Mg–Si system, and we include the binary Al–Mg and Al–Si alloys mainly to help isolate the ternary-specific features in the μSR data. The processes occurring in the binary subsystems is definitely still worth investigating by their own right, seeing that they are used as alloys for many applications where high strength is not required [2]. No precipitation has been observed in annealed Al–Mg alloys, while diamond Si particles precipitate in the Al–Si system, without increasing the hardness significantly [16]. These particles also form in over-aged Si-rich Al–Mg–Si alloys [13]. Very dilute alloys have been probed with μSR earlier, and small additions of Si, Mg and Cu were found to greatly affect the muon kinetics [17]. Our previous work on the Al–Mg–Si system revealed the presence of a muon trapping peak corresponding to clustering/precipitation [18]. By analysing more conditions, and including binary alloys, we aim to improve our understanding of the interactions between muons and precipitates in Al–Mg–Si alloys. The main goal of the current work is to establish a connection between muon trapping rates and the microstructure of materials as found from TEM and APT

studies.

We will dive further into the theory of muons and their interactions with samples in the next section. Sections 3 and 4 explain the procedures of the experiments and the analysis of μSR data. Results from various experiments on Al(–Mg)(–Si) alloys are presented in Sec. 5. Some mechanisms of muon trapping are proposed in the discussion part (Sec. 6), and are used to infer the behavior of vacancies during heat treatment of Al alloys, leading up to the conclusions in Sec. 7.

2. Theory

Like electrons, muons are elementary particles in the lepton family. As in most muon spin research [19], we use positively charged muons, since the negatively charged variant has a material-dependent lifetime. The lifetime of a positive muon always has an average value of 2.197 µs. The muon decays to a positron and two neutrinos:

$$\mu^+ \rightarrow e^+ + \nu_e + \bar{\nu}_\mu. \tag{2}$$

The direction of motion for the positron is asymmetric with respect to the muon spin, a fact which μSR measurements depend on [20]. The exact distribution for the emission angle with respect to the muon spin, θ, is

$$p(\theta) = 1 + A\cos\theta, \tag{3}$$

where A is an asymmetry parameter dependent on the experimental setup. Positrons are detected in the backward and forward directions with respect to the initial muon spin. From the positron counts N_b (backward) and N_f (forward), the muon spin asymmetry $G(t)$ is calculated:

$$G(t) = \frac{N_\mathrm{f} - \alpha N_\mathrm{b}}{N_\mathrm{f} + \alpha N_\mathrm{b}}, \tag{4}$$

where t is the time after muon implantation and the parameter α compensates for differences in distance between the sample and the two detectors. The asymmetry is often expressed through a normalized *relaxation function* $g(t) = G(t)/A$, with the property $g(0) = 1$.

Larmor precession of the muon spin in the local magnetic fields $\mathbf{B}$ can be calculated using matrix multiplication and trigonometric functions of ωt, where $\omega = \gamma_\mu \|\mathbf{B}\|$, with γ_μ being the gyromagnetic ratio of the muon. A

muon in a static magnetic field has a trivial spin relaxation [21]. For an ensemble of interstitially diffusing muons, the magnetic field changes upon muon site transitions. An abrupt transition between uncorrelated fields is a good approximation, and is applied in the strong-collision model [21]. Even when this simplified model is used, the general problem of spin relaxation for muons with site-dependent diffusion rates is not analytically solvable. However, the relaxation function can be found by integral [22] or differential equations [23] for some specific cases.

An important feature of any model applied to Al alloys is the inclusion of muon trapping by defects. The concentration of a defect type and its binding energy with muons manifests itself in the measured relaxation function. The spin relaxation behavior in aluminium has a much more complicated temperature variation than that of e.g. copper [24]. This is due to very fast muon diffusion and trapping by vacancies and trace elements, which are heavily temperature-dependent processes [25]. Our method for calculating relaxation functions is described in Sec. 4.

3. Experimental

Samples of pure Al (99.99 %), Al–Mg, Al–Si, and Al–Mg–Si alloys were used in the μSR experiments. The material was cast and rolled to 1 mm sheets at the University of Toyama. The sample dimensions were 25 mm × 25 mm × 1 mm. A SHT of 1 hour at 575 °C and subsequent quenching in ice water was conducted for all samples, before one of three heat treatment procedures were performed:

1. μSR measurement directly (approx. 15 minutes) after quenching, which we call *as-quenched* (AQ) conditions.
2. Some time, typically days/months of storage at room temperature (RT) before μSR measurements.
3. Annealing for 1000 minutes ($\approx$ 16 h) at some specified temperature before μSR measurements.

In the results section, samples are denoted based on their atomic (molar) fraction of solute, e.g. Al–0.5 % Mg. The Al–Mg–Si alloy we have used has 1.6 % solute and twice as much Mg as Si, and is thus referred to through its semi-binary composition Al–1.6 % Mg_2Si. The annealing temperatures are always given in °C, while the sample temperatures during measurements are always in K. Table 1 displays all the conditions used in this work.

Table 1: Compositions (columns) and heat treatments (rows) of the 16 samples used in the current μSR measurements. AQ: as-quenched, RT: room temperature. Conditions with * were analysed in a previous publication [18] and are included here for comparisons in a broader context.

Composition (at.%), balance is Al	1.6 % Mg_2Si	0.5 % Mg	0.5 % Si	0.01 % impurities
1. AQ	Yes* (2)	Yes	Yes	
2a. RT for $\approx$ 2 weeks	Yes*	Yes	Yes	
2b. RT for $>$ 2 months	Yes*			Yes*
3a. 70/100/150 °C for 1000 min	Yes*/Yes*/Yes			
3b. 200 °C for 1000 min	Yes*	Yes	Yes	
3c. RT for 7d + 100 °C for 1000 min	Yes			

The μSR experiments were conducted at the RIKEN-RAL Muon Facility in Oxfordshire, UK [26]. We used the ARGUS muon spectrometer, which is equipped with a total of 192 positron detectors in annular forward and backward arrays, covering a 25 % solid angle. A helium cryostat was used to control the temperature of the samples during the measurements. To capture the muon diffusion kinetics in a broad temperature region, we measured muon spin relaxation functions while heating stepwise from 20 K to 300 K. 20–60 million positron detections (*events*) were recorded at 12–20 temperature points for all conditions.

Four of the samples, annealed at 150 °C and above, were prepared (as in e.g. [27]) for transmission electron microscopy (TEM) investigations of the precipitate microstructure. Bright-field images recorded on film with a Philips LaB_6 CM30 TEM were used for this analysis. The microscope was operated using an acceleration voltage of 150 kV.

4. Data analysis and simulations

Apart from direct visual comparison, our method of choice for interpreting relaxation functions is comparing them to a Monte Carlo (MC) sim-

ulation. An indeterministic simulation is appropriate, since diffusion, trapping/detrapping by defects, the magnetic field at muon sites and muon decay are all stochastic processes/variables. The magnetic field vectors are Gaussian distributed with a standard deviation Δ/γ_μ, where Δ is the *dipolar width*, proportional to the strength of the magnetic field. An ensemble of 60 million muons are simulated, varying four parameters: the dipolar width Δ, the trapping/detrapping rates ν_t and ν_d and the fraction of initially trapped muons p_0. In defect-free locations, the diffusion rate of muons is practically infinite in comparison to their depolarization rate [14, 22], so our model neglects spin relaxation unless the muon is trapped. Temperature is not included explicitly in the simulations, but manifests itself in the thermodynamics, which is controlled through the fitting parameters ν_t and ν_d. The decay of a muon is calculated with Eq. (3). Forward/backward positrons are counted, and put into one of 2000 bins based on their lifetime, as in the experiments.

Simulated relaxation functions are fitted to the experimental ones by running through a database of fitting parameters and associated functions. Each experimental time bin has a calculated error $\epsilon(t)$ in spin relaxation (calculated by assuming the detected muons to follow a Poisson distribution). These errors are used as fitting weights, $w(t) = \epsilon(t)^{-2}$. Fitting parameters are estimated as an average over all the simulated relaxation functions, using the total fitting error as weight: $W_i = E_i^{-2}$ for simulated function i. This reduces the scatter in the results from simply using the parameters of a single best-fit simulated function. Similarly, the errors in the fitting parameters are estimated from a weighted standard deviation. For tests of the fitting procedure, see Sec. 5.1.

It is desirable to predict the trapping sites for muons based on their binding energies to simple point defects. Due to restrictions in the software used for energy calculations, we use a hydrogen ion (a proton) as a crude model for a positive muon in Al. The hydrogen ion H^+ has the same charge as μ^+, and a 9 times higher mass. Both tend to localize at interstitial sites in Al. In particular, muons prefer sites with tetrahedral symmetry at temperatures above ≈ 15 K [24]. Muons do not form muonium (a bound muon–electron system) in metals, and hydrogen stays ionic by analogy. For simplicity, we nonetheless refer to it by H in the further. To find the binding energy between H and solute atoms/vacancies, we employ the Vienna ab initio simulations package (VASP) [28, 29], which performs quantum mechanical energy calculations using density functional theory (DFT) [30, 31]. The supercell of the model system consists of 216 Al atoms on an fcc lattice, where one atom is

replaced by Mg, Si or a vacancy, and a H atom is introduced at a neighboring interstitial site. The binding energy between H and a substitutional defect X is calculated as follows:

$$E(\text{H–}X) = E(215\text{Al}+\text{H}+X) - E(216\text{Al}+\text{H}) - E(215\text{Al}+X) + E(216\text{Al}). \quad (5)$$

For more computational details, we refer to the similar calculations in [11].

5. Results

5.1. Reproducibility of measurements

As a check of the consistency of our μSR measurements and of the fitting to simulated data, we have run two equal experiments on the Al–1.6 % Mg_2Si alloy in an as-quenched condition. After quenching, the samples were prepared for the measurements, which required keeping them at RT for ≈ 15 min before cooling down to 20 K. The number of events measured and the number of temperature points were lower in the second run, leading to shorter storage at e.g. 300 K inside the spectrometer. As longer time at higher temperatures promotes atomic clustering, this creates minor differences in microstructure between the two conditions, but these are most likely smaller than the combined errors of experiment and fitting. Therefore, the differences in spin relaxation is bound to indicate the reproducibility/accuracy of zero-field μSR measurements as applied to Al alloys. Overlay plots of the relaxation functions for all measurement temperatures are presented in Fig. 1. The initial asymmetry (at time $t = 0$) is slightly different due to unavoidable differences in the experimental setup. This effect is taken into account in the analysis. Otherwise, it is difficult to observe any differences in the relaxation functions by eye.

Figure 2 shows the fitting parameters we obtain when comparing the data in Fig. 1 to simulated relaxation functions. The greatest deviations are in the fraction of initially trapped muons and the trapping rates, suggesting that these parameters cause the least variation to the relaxation functions when altered. The trapping rate is difficult to estimate at low temperatures because the relatively slow kinetics do not bring the system near an equilibrium before the muons decay. Regardless of this, we mainly use the trapping rate ν_t to compare conditions in the further, as it is readily interpretable in terms of defect content. Figures 1 and 2 shows that the reproducicbility of the experiments is reasonable and that the error in ν_t is well estimated.

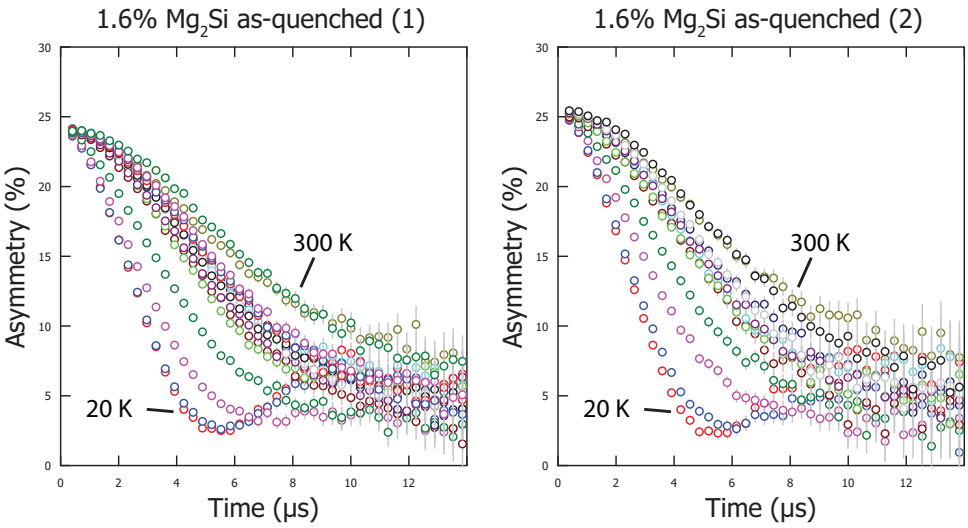

Figure 1: Overlays of relaxation functions measured at temperatures from 20 K to 300 K. Both samples come straight from quenching after SHT, and are compared to check the reproducibility of the μSR experiments. The set of colors do not correspond to the same temperatures in both cases.

In connection to this uncertainty analysis, we note that the 100 °C annealed and 15 days RT stored Al–1.6 % Mg_2Si samples had incorrect fitting parameters (e.g. too low ν_t) in a previous publication [18]. The cause of the errors was related to the experimental setup, and has been corrected for in this paper.

5.2. Binary alloys and their relationship to Al and Al–Mg–Si

Six experiments with binary alloys were conducted, with Al–0.5 % Mg and Al–0.5 % Si in as-quenched, RT stored and annealed conditions. The trapping rates are shown separately for the two systems in Fig. 3. It becomes immediately obvious that Mg and Si atoms affect muons very differently. We note the following trapping rate characteristics for Al–Mg:

- Heat treatment does not change the muon behavior much in Al–Mg alloys.
- There is a remarkable coincidence of Al–Mg and Al–Mg–Si at temperatures up to 120 K, despite a big difference in Mg content.

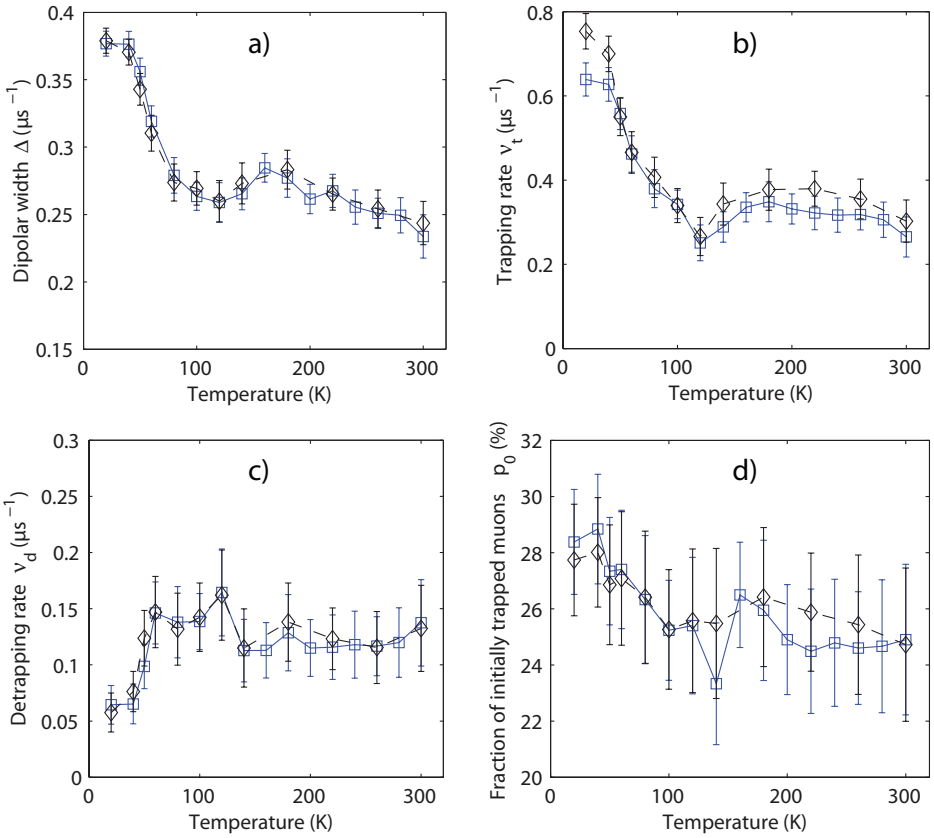

Figure 2: Fitting parameters for the alloy with 1.6 % Mg_2Si, directly after quenching from SHT. Two identical experiments. The first experiment (Fig. 1(a)) is indicated by squares connected by a whole blue line.

- RT stored and as-quenched samples have a higher trapping rate than pure Al at temperatures 240–300 K. This is not the case for the sample annealed at 200 °C.
- All Al–Mg conditions have a trapping peak at 160 K, for which we can currently provide no explanation.

Correspondingly, for Al–Si:

- The muon behavior in annealed and RT stored samples is very similar to pure Al, excluding only the lowest temperatures.

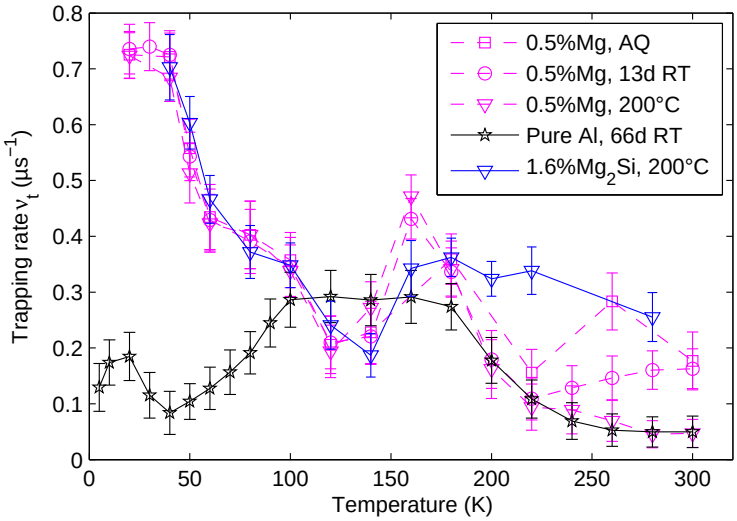

(a)

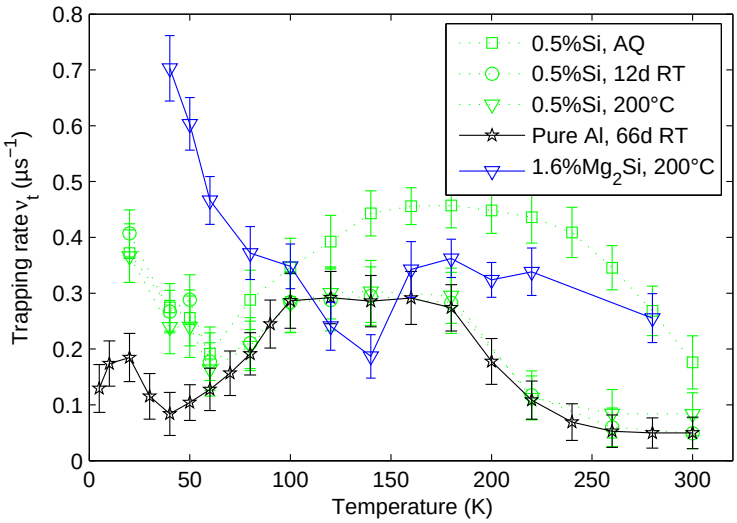

(b)

Figure 3: Calculated trapping rates in binary alloys, (a) Al–Mg and (b) Al–Si, compared to pure Al and the Al–Mg–Si alloy. The samples are either as-quenched (AQ), room temperature (RT) stored for approx. two weeks, or annealed for 1000 min at 200 °C after SHT.

- Only when measuring directly after quenching from SHT, we observe a significant difference at high temperatures. The extended peak from 100 K to 250 K is similar to peaks previously observed in Al–Mg–Si for all kinds of heat treatments (see [18] and Figs. 5 and 6).

TEM images of the annealed conditions were obtained, and are presented in Fig. 4. Some dislocations are observed in both samples, with a slightly

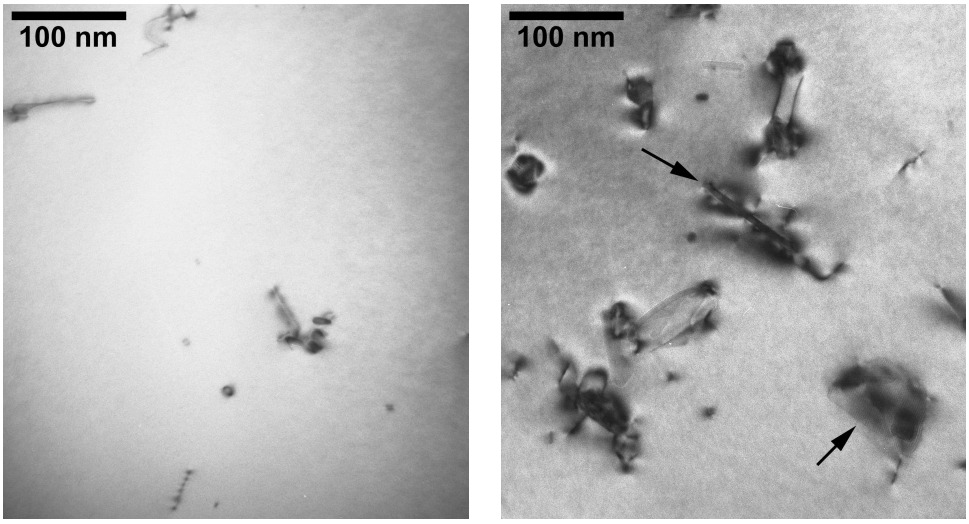

(a) (b)

Figure 4: TEM images of binary alloys annealed for at 200 °C for 1000 minutes after SHT. Both are viewed in the $[001]_{\mathrm{Al}}$ direction. (a) Al–0.5 % Mg. (b) Al–0.5 % Si. Two of several diamond Si particles are indicated by arrows in (b).

higher concentration in Al–Si. Diamond Si particles are also present in Al–Si. They mainly have a plate morphology with typical size 70 nm×70 nm×7 nm, seen both edge-on and as Moiré patterns in Fig. 4(b). No particles are observed in Al–Mg.

5.3. Al–Mg–Si alloys with RT storage before annealing

Motivated by results from APT [6], we have conducted μSR experiments on the ternary Al–1.6 % Mg_2Si alloy annealed for 1000 min at 100 °C with and without RT storage between SHT and this annealing. Figure 5 shows the calculated trapping rates of the two conditions, as well as a condition with

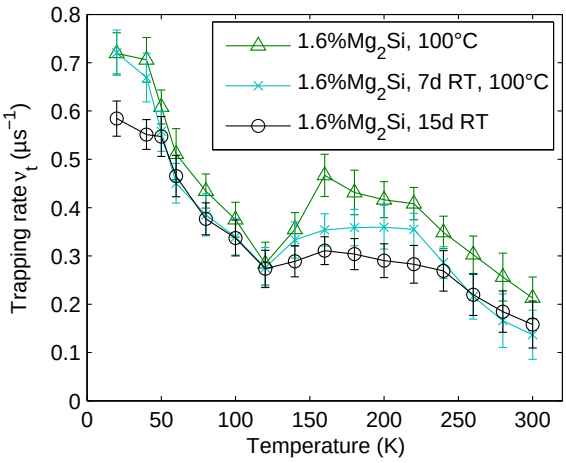

Figure 5: Trapping rates of an annealed Al–1.6 % Mg_2Si alloy, with/without a week of RT storage between SHT and the annealing. A sample with only two weeks of RT storage after SHT is included for comparison.

15 days of RT storage (and no annealing) for comparison. We see that the annealed samples follow each other until a temperature of 120 K is reached, after which the trapping is consistently lower in the sample with RT storage. The sample with only RT storage lies even lower in this region.

In addition to having a diminished high temperature trapping peak, the exclusively RT stored sample also lie below the annealed samples at low measurement temperatures. This is observed for all as-quenched and RT stored samples, and is discussed in Sec. 6.1.

5.4. Influence of annealing temperature on trapping rates in Al–Mg–Si alloys

Adding to the conditions previously investigated [18], we have data from a set of Al–1.6 % Mg_2Si alloys annealed for 1000 min at four different temperatures. Higher temperatures will bring the microstructure in the material further along the precipitation sequence in Eq. (1). The results of this study are shown as muon trapping rates in Fig. 6. Annealing at 70 °C, 100 °C and 150 °C gives a very similar muon behavior, with the characteristic peak above 120 K higher than in as-quenched and RT stored conditions, which are also shown in the figure. Annealing at 200 °C reduces the trapping rate to the as-quenched level. Since RT storage is equivalent to annealing the sample at

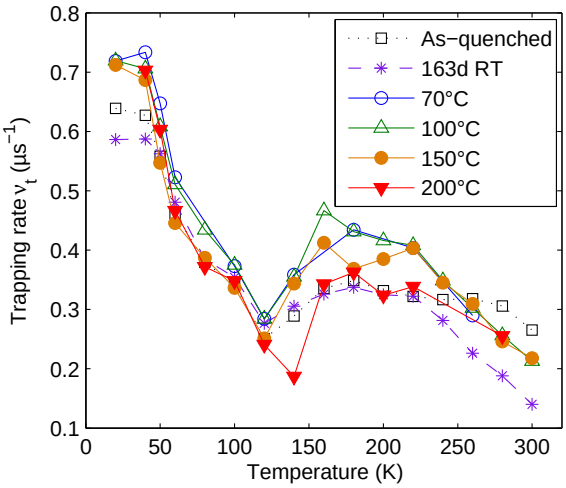

Figure 6: Muon trapping rates in Al–1.6 % Mg_2Si, annealed for 1000 min at different temperatures. Samples which are RT stored and as-quenched from SHT are included for comparison. See Fig. 5 for approximate error bars.

≈ 20 °C for a very long time, we see the biggest changes in the transitions 20 °C $\rightarrow$ 70 °C and 150 °C $\rightarrow$ 200 °C.

TEM images of the microstructure in the alloys annealed at 150 °C and 200 °C are shown in Fig. 7. The 150 °C annealed sample has a fine microstructure of β'' precipitates and their precursors (pre-β'' GP-zones, see [32]). Annealing at 200 °C is seen to produce a coarser microstructure. As the alloy begins to over-age, the precipitate types change from β'' to larger β' and other less coherent phases (see [27] for more detailed TEM studies of a similar alloy annealed at 200 °C). In some cases, clusters formed during annealing at 70–100 °C are also observable by TEM, see e.g. [33]. We have not attempted such analysis in this work, and refer instead to APT results on similar conditions when discussing low-temperature annealing in Sec. 6.

5.5. Calculations of muon binding energy

Binding energies between hydrogen and substitutional defects in Al–Mg–Si alloys were calculated as explained in Sec. 4, and are displayed in Table 2. H at an octahedral site in pure Al and H as a substitutional defect are included for completeness. The hydrogen ion H^+ has a larger mass than a muon μ^+, and thus different binding energies, but the numbers should follow

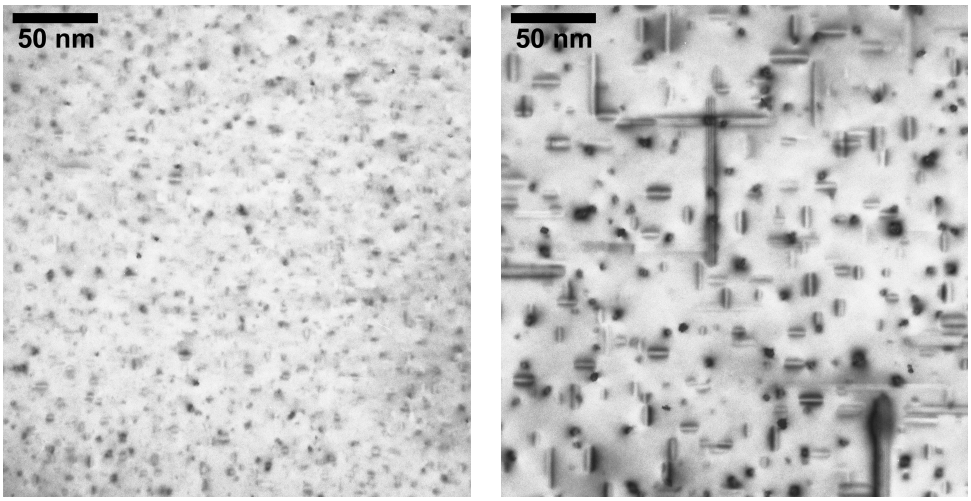

(a) (b)

Figure 7: TEM images of Al–1.6 % Mg_2Si annealed for 1000 minutes at temperatures (a) 150 °C and (b) 200 °C after SHT. Both are viewed in the $[001]_{Al}$ direction, and the precipitates are aligned along $\langle 001 \rangle_{Al}$ directions.

a similar trend for muons. We see that substitutional and octahedral sites are very unfavorable for a hydrogen atom. The main result is that the binding energy of hydrogen/muons to substitutional defects is sorted as Si < Mg < vacancy.

Measuring binding energies using μSR is a challenge because of the complexity of the physics involved. Most regions of a typical Arrhenius plot do not look linear, meaning that simple Boltzmann kinetics is insufficient to describe the real situation. High-temperature tails create reasonably linear Arrhenius plots, as shown in Fig. 8 with a linear fit in the temperature range 200–300 K. The two selected conditions are Al–Mg and Al–Mg–Si alloys, only the last of which should have any solute clustering dynamics. The linear fit gives activation energies of 0.0199 eV (Al–0.5 % Mg, 1000 min at 200 °C) and 0.0633 eV (Al–1.6 % Mg_2Si, 163 days at RT). This can be interpreted as binding energies for a high-temperature muon trap, with seemingly very different nature in the two cases. The activation energy for the low-temperature peak (20–80 K) of the same Al–1.6 % Mg_2Si condition was measured to 0.0069 eV. The low-temperature trap is thus considerably easier to escape from.

Table 2: Binding energies between hydrogen and point defects in Al–Mg–Si alloys as calculated by DFT and Eq. 5. Tetr. and Oct. mean tetrahedral and octahedral interstitial sites, respectively. The energy of hydrogen at a tetrahedral site in pure Al is always used as a reference.

Hydrogen site	Energy (eV)
Tetr. next to Mg	−0.1298
Tetr. next to Si	−0.0318
Tetr. next to vacancy	−0.3109
Subst. (inside vacancy)	0.4965
Oct. in pure Al	0.2560

6. Discussion

6.1. Muon trapping in Al(–Mg)(–Si)

We focus here on the bonds formed between muons and various lattice defects in aluminium, which has been shown to greatly influence the measured muon spin relaxation functions.

At low temperatures, Al–Mg has a much higher trapping peak than Al–Si (Fig. 3), leading to a clear conclusion: Mg–μ^+ bonds are stronger than Si–μ^+ bonds. This is supported by the DFT results for hydrogen–solute bonds in Table 2, and can be qualitatively explained in terms of the lower number of valence electrons in Mg relative to both Al and Si [17]. The height of the low-temperature trapping peak is the same for Al–0.5 % Mg and Al–1.6 % Mg_2Si (roughly twice the amount of Mg atoms). It seems the Mg–μ^+ trapping kinetics reach a point of saturation at low concentrations of Mg. As-quenched Al–Si has a large trapping peak above 60 K, which disappears with any heat treatment, including storage at RT. Al–Mg has a radically different behavior, losing its high-temperature muon trapping only after annealing. A simple explanation is that Al–Mg needs annealing to get rid of its vacancies, while Al–Si gets them out already during room temperature storage. Vacancies have certainly been found to diffuse slowly near Mg atoms [34]. The trapping site in as-quenched Al–Si can be small clusters of Si and vacancies, judging by the favorability of such bonds [35, 36]. If this interpretation is correct, the vacancies leave the clusters and disappear from the material during weeks at RT. Large, incoherent diamond Si particles have apparently no effect on the muon behavior, judging from the lack of differences in muon trapping rate between RT stored and annealed samples in Fig. 3(b).

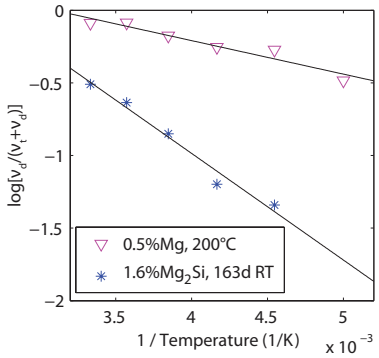

Figure 8: Arrhenius plot, showing the logarithm of the equilibrium fraction of free (de-trapped) muons. The selected conditions are Al–0.5 % Mg annealed at 200 °C for 1000 min and Al–1.6 % Mg_2Si stored at room temperature for 163 days. Measurement temperatures are in the range 200–300 K.

Figure 5 shows that there is less muon trapping at the previously identified "cluster trapping peak" [18] in annealed samples if they have been RT stored before the annealing. According to APT findings, the sample with direct annealing has approx. 5 times more clusters than the sample with RT storage before the annealing [6]. It was shown that these are "good" clusters, being more compact (solute-rich) and having a Mg/Si ratio close to 1. The cluster sizes do not change between the two conditions. There should not be other differences between the conditions with and without RT storage, and what we observe with μSR are thus quite certainly caused by the composition, vacancy content and/or concentration of solute clusters.

The influence of microstructure on the μSR signal can be further deduced by the annealing temperature experiments on the Al–Mg–Si alloy (Fig. 6). A transition between a cluster-dominated microstructure (70 °C annealing) to a mix of clusters and small, coherent precipitates give no apparent difference in muon kinetics. However, annealing at 200 °C gives a lower trapping rate at measurement temperatures around 200 K. The annealing transforms some clusters/precipitates into larger, less coherent precipitates while some of them dissolve, reducing the overall precipitate number density. Alloy conditions in early stages of the precipitation sequence [Eq. (1)] are apparently most efficient at trapping muons.

The insight gained from the experiments in this work is attempted con-

densed in Fig. 9. Each nano-sized defect in a material will give a "signature" in the muon trapping behavior, which is characteristic of some kind of defect. The lower black line is what we expect the trapping rate to look like

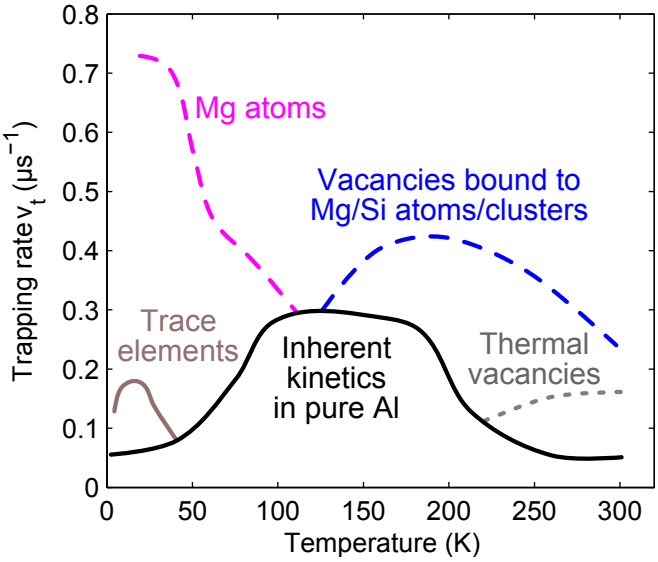

Figure 9: Schematic of the signatures of defects on the muon trapping rate, as understood from Figs. 3, 5 and 6.

in 100 % pure Al. Its inherent muon kinetics might include subtle effects of dislocations and grain boundaries. Trace/impurity elements (brown line) and alloying elements (pink, dashed line), especially Mg (and Cu [17]), trap muons at low temperature. The trapping at temperatures close to 300 K (gray, dotted line) is observed in the non-annealed Al–0.5 % Mg sample. As-quenched Al–Mg–Si samples also have an elevated trapping in this region, and our previous in situ studies [15] show that this is also the case for as-quenched pure Al. A non-equilibrium (thermal) vacancy concentration, introduced through SHT, is most likely to be responsible. The trapping peak around 200 K (blue, dashed line) was previously associated with clustering/precipitation [18]. It is the most interesting feature of the curves as it is observed exclusively in Al–Mg–Si samples and as-quenched Al–Si. We hypothesize that the trapping sites of this peak are vacancies in Mg/Si–rich environments, in particular vacancies which are themselves trapped by clus-

ters or precipitate phases. The muon trapping potential of such vacancies has not been investigated, but it is likely to be close to that of free vacancies in Al, given the much weaker muon (or hydrogen) interaction with Mg and Si atoms (see Table 2).

Figures 5 and 6 show that as-quenched and RT stored Al–1.6 % Mg_2Si samples have a reduced trapping rate at low temperatures as compared to Al–Mg and annealed Al–Mg–Si samples. Why Mg atoms should have a lower muon trapping potential in these conditions is not clear at this point, but it might be related to the change in solute atom distribution through clustering.

6.2. Vacancy behavior during heat treatment

According to the calculated binding energies in Table 2, muons prefer to be located at interstitial sites next to a vacancy, but the concentration of vacancies is always very low compared to e.g. solute atoms. A high temperature is required to increase the muon diffusivity and break muons loose from other defects so that they are able to find vacancies to bind to. Assuming the interpretation of the 200 K-peak from the previous subsection (muon trapping by vacancies in solute-rich environments), we can draw some conclusions about the behavior of vacancies in Al alloys.

Around 200 K, muons seem to have a strong bond with Si-vacancy clusters formed after quenching from SHT (see Fig. 3(b)) After 12 days at RT, the trapping peak disappears, while it lasts indefinitely in Al–Mg–Si alloys, regardless of heat treatment (Figs. 5 and 6). This means that with the heat treatments done in this work, there are always some vacancies trapped in clusters and possibly early precipitate phases. The total number of vacancies inside Al–Mg–Si is then always greater than in pure Al, when the materials are treated equally. Figure 10 shows the average trapping rate in the temperature interval 140–240 K for all Al–1.6 % Mg_2Si conditions in Figs. 5 and 6. The typical microstructure for each condition is included, based on the current TEM analysis and previous analysis with TEM and APT of similar conditions [5, 10, 6, 27, 32]. The trapping maximum at an annealing temperature of 100 °C does not correspond directly to a maximum in any known microstructural parameter. In light of the preceding discussion, we nevertheless suggest that the vacancy concentration inside clusters/precipitates peaks at this point. It is possible that the ability of a precipitate to trap vacancies decreases when its coherency with Al decreases, and that it is also affected by the precipitate composition.

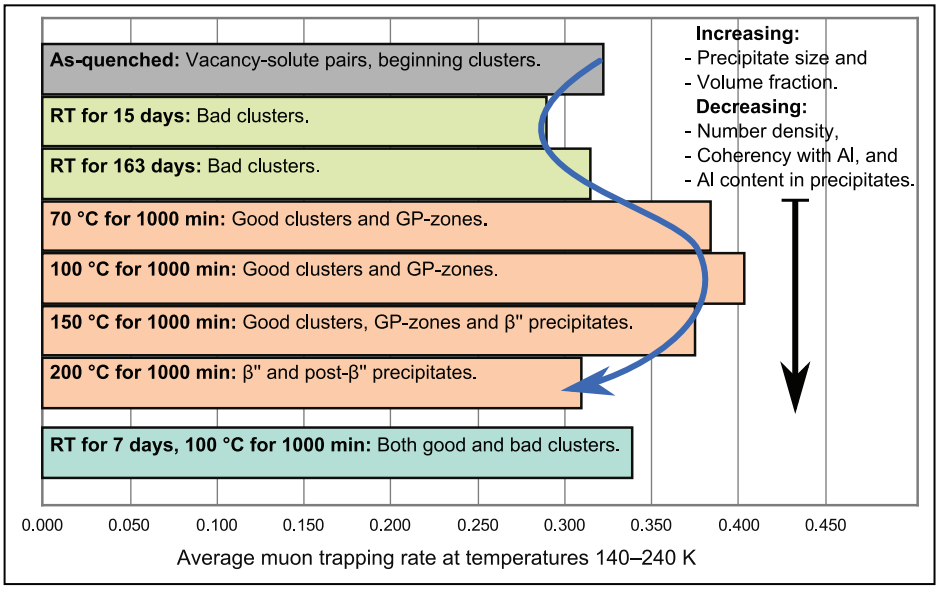

Figure 10: Qualitative summary of the main trapping rate peaks of the Al–1.6 % Mg_2Si samples in Figs. 5 and 6. The expected properties of the cluster/precipitate microstructure is given for each condition. Guinier–Preston (GP)-zones are periodic solute-rich structures with Mg and Si atoms still at Al-fcc positions [32].

Although no current technique can probe the exact structure of nanoclusters, the good clusters might have a pre-β'' Guinier–Preston (GP)-zone [32] structure at the moment they nucleate from the Al matrix. An indication of the presence of good and bad clusters is noted down for each condition in Fig. 10, showing a good correspondence between good cluster content and muon trapping rate. Our interpretation is that muon-trapping vacancies reside in these clusters, which retain an Al-fcc structure. Once they transform into β'' and other phases, they lose their ability to contain vacancies, which lowers the muon trapping rate.

Diamond Si particles do not affect muon kinetics, and therefore do not trap vacancies. The equilibrium phase β in the Al–Mg–Si system, with composition Mg_2Si, forms as big, incoherent cubes, similar to diamond Si. If β also does not trap vacancies, the blue peak in Fig. 9 should not be present in a sample containing only β. Such a very over-aged Al–1.6 % Mg_2Si alloy should be studied in the future, as it could be an interesting test of our interpretation.

7. Conclusion

An extensive study on the muon behavior in Al–Mg–Si, Al–Mg, Al–Si and pure aluminium has been conducted. Heat treatments were designed for the investigation of diffusion and clustering phenomena in different stages of the precipitation, which is crucial to the properties of commercial Al–Mg–Si alloys. We have shed light on some important findings regarding the muon trapping in the materials and its interpretation in terms of (sub-)nanometer-sized defect content. In particular, muons were found to prefer the company of Mg atoms over Si atoms, as was predicted by density functional theory calculations. The vacancy kinetics are surprisingly different in the two binary alloys. In Al–Si, Si–vacancy clusters are forming, but vacancies still leave the material faster in Al–Si than in Al–Mg. A characteristic peak in the muon trapping rate is seen in Al–Mg–Si in the temperature range 100–250 K, regardless of heat treatment. Since there are many steps of reasoning in our analysis of this peak, we summarize it here in a bottom-up order:

1. Annealing an Al–1.6 % Mg_2Si alloy at 70–150 °C for 1000 minutes produces a fine microstructure of "good" (see Sec. 6.2) clusters and GP-zones with Mg and Si atoms retaining Al-fcc positions. This has been well established by numerous earlier APT and TEM investigations.
2. These structures trap a higher amount of vacancies than bulk Al and precipitates with a non-fcc structure. This is the main hypothesis of this paper.
3. Muon–vacancy bonds have a high binding energy, as found by the current DFT calculations as well as μSR experiments on Al(–Mg)(–Si) alloys.
4. The trapping of muons by vacancies inside good clusters/GP-zones occurs when the alloy sample is kept at temperatures in the range 100–250 K.
5. This trapping increases the muon depolarization rate. The steepness of the relaxation functions (Fig. 1) at the temperatures in question can thus be linked to the presence of good clusters/GP-zones.

Two transitions are observed in the muon trapping rate when changing the annealing temperature: an increase between room temperature and 70 °C and a decrease between 150 °C and 200 °C. These transitions indicate the appearance of good clusters/GP-zones, and their disappearance associated with over-aging, respectively.

Muon spin relaxation has proved to be sensitive to very small concentrations of defects important for diffusional phase transformations. It is complimentary to more established techniques such as TEM, APT and DSC, and has potential to aid our understanding and development of aluminium alloys.

Acknowledgements

This work was financially supported by The Research Council of Norway and Norsk Hydro via project no. 193619, The Norwegian–Japanese Al–Mg–Si Alloy Precipitation Project. The authors kindly acknowledge Dr. Flemming J. H. Ehlers for his contributions to the calculations of hydrogen binding energies.

[1] Kubo, R., Toyabe, T.. In: Blinc, R., editor. Magnetic Resonance and Relaxation. Amsterdam: North-Holland; 1967, p. 810.

[2] Davis, J.R., editor. Aluminum and Aluminum Alloys. ASM Specialty Handbook; ASM International; 1993.

[3] Ferragut, R., Dupasquier, A., Macchi, C.E., Somoza, A., Lumley, R.N., Polmear, I.J.. Scripta Mater 2009;60(3):137–140.

[4] Banhart, J., Lay, M.D.H., Chang, C.S.T., Hill, A.J.. Phys Rev B 2011;83:014101.

[5] Serizawa, A., Hirosawa, S., Sato, T.. Met Mater Trans A 2008;39:243–251.

[6] Torsæter, M., Hasting, H.S., Lefebvre, W., Marioara, C.D., Walmsley, J.C., Andersen, S.J., et al. J Appl Phys 2010;108(7):073527.

[7] De Geuser, F., Lefebvre, W., Blavette, D.. Phil Mag Lett 2006;86(4):227–234.

[8] Zhen, L., Kang, S.. Materials Letters 1998;37(6):349–353.

[9] Chang, C.S.T., Banhart, J.. Met Mater Trans A 2011;42:1960–1964.

[10] Torsæter, M.. Quantitative studies of clustering and precipitation in Al–Mg–Si(–Cu) alloys. Ph.D. thesis; Norwegian University of Science and Technology, Department of Physics; 2011.

[11] Martinsen, F.A., Ehlers, F.J.H., Torsæter, M., Holmestad, R.. Acta Materialia 2012;60(17):6091–6101.

[12] Zandbergen, H.W., Andersen, S.J., Jansen, J.. Science 1997;277(5330):1221–1225.

[13] Marioara, C.D., Andersen, S.J., Zandbergen, H., Holmestad, R.. Metallurgical and Materials Transactions A 2005;36:691–702.

[14] Kehr, K.W., Richter, D., Welter, J.M., Hartmann, O., Karlsson, E., Norlin, L.O., et al. Phys Rev B 1982;26:567–590.

[15] Wenner, S., Matsuda, K., Nishimura, K., Banhart, J., Matsuzaki, T., Tomono, D., et al. Muon spin relaxation and positron annihilation spectroscopy studies of natural ageing in Al–Mg–Si alloys. In: Heiland, W., Rollett, A.D., Cassada, W., editors. 13th International Conference on Aluminum Alloys. Wiley; 2012, p. 37–42.

[16] Marioara, C.D., Andersen, S.J., Birkeland, A., Holmestad, R.. J Mater Sci 2008;43:4962–4971.

[17] Doyama, M., Hatano, T., Natsui, T., Suzuki, Y., Uemura, Y.J., Yamazaki, T., et al. Hyperfine Interactions 1984;17:225–229.

[18] Wenner, S., Holmestad, R., Matsuda, K., Nishimura, K., Matsuzaki, T., Tomono, D., et al. Phys Rev B 2012;86:104201.

[19] Yaouanc, A., De Réotier, P.D.. Muon Spin Rotation, Relaxation, and Resonance: Applications to Condensed Matter. Oxford University Press; 2011.

[20] Garwin, R.L., Lederman, L.M., Weinrich, M.. Phys Rev 1957;105:1415–1417.

[21] Hayano, R.S., Uemura, Y.J., Imazato, J., Nishida, N., Yamazaki, T., Kubo, R.. Phys Rev B 1979;20:850–859.

[22] Boekema, C., Heffner, R.H., Hutson, R.L., Leon, M., Schillaci, M.E., Kossler, W.J., et al. Phys Rev B 1982;26:2341–2348.

[23] Borghini, M., Niinikoski, T.O., Soulié, J.C., Hartmann, O., Karlsson, E., Norlin, L.O., et al. Phys Rev Lett 1978;40:1723–1726.

[24] Hartmann, O., Karlsson, E., Norlin, L.O., Niinikoski, T.O., Kehr, K.W., Richter, D., et al. Phys Rev Lett 1980;44:337–340.

[25] Schenck, A.. Muon spin rotation spectroscopy. The University of California; 1985.

[26] Matsuzaki, T., Ishida, K., Nagamine, K., Watanabe, I., Eaton, G.H., Williams, W.G.. Nuclear Instruments and Methods A 2001;465(2–3):365–383.

[27] Wenner, S., Marioara, C.D., Andersen, S.J., Holmestad, R.. Int J Mater Res 2012;103:948–954.

[28] Kresse, G., Hafner, J.. Phys Rev B 1993;47:558–561.

[29] Kresse, G., Furthmüller, J.. Comp Mater Sci 1996;6(1):15–50.

[30] Hohenberg, P., Kohn, W.. Phys Rev 1964;136:B864–B871.

[31] Kohn, W., Sham, L.J.. Phys Rev 1965;140:A1133–A1138.

[32] Marioara, C.D., Andersen, S.J., Jansen, J., Zandbergen, H.W.. Acta Materialia 2001;49(2):321–328.

[33] Murayama, M., Hono, K.. Acta Mater 1999;47(5):1537–1548.

[34] Liu, M., Yan, Y., Liang, Z., Chang, C.S.T., Banhart, J.. Influence of Mg and Si on cluster formation in Al-Mg-Si alloys studied by positron annihilation lifetime spectroscopy. In: Heiland, W., Rollett, A.D., Cassada, W., editors. 13th International Conference on Aluminum Alloys. Wiley; 2012, p. 1131–1136.

[35] Kim, S.M., Buyers, W.J.L., Martel, P., Hood, G.M.. J Phys F: Met Phys 1974;4(3):343.

[36] Hirosawa, S., Nakamura, F., Sato, T.. Mater Sci Forum 2007;561–565:283–286.